A Modelling and XANES Study on the Structure of the Amorphous $Fe_{90}Zr_{10}$-Alloy

P. Kizler, P. Lamparter, and S. Steeb

Max-Planck-Institut für Metallforschung, Institut für Werkstoffwissenschaften, Stuttgart, F.R.G.

Z. Naturforsch. **44a**, 7–14 (1989); received October 17, 1988

It is shown that it is possible to set up a structural model for the amorphous $Fe_{90}Zr_{10}$-alloy which is in agreement both with diffraction and XANES data, the latter being sensitive to higher than binary correlations.

1. Introduction

Up to now, two investigations on the structure of amorphous $Fe_{90}Zr_{10}$-alloys were published. In [1] conventional X-ray diffraction and in [2] the method of anomalous dispersion of X-rays was applied. This way the total pair correlation function and the partial Fe–Fe- and Fe–Zr-correlation functions were determined.

Further insight into the structure is expected from higher than binary correlation functions [3]. One method, which is sensitive to higher order correlations, is the investigation of the X-ray absorption near edge structure, XANES. Because of electron multiple scattering processes, taking place in this energy range, XANES depends to some extent on the correlation of three or more atoms [4].

In the present work, modelling was done and XANES-predictions for different models were obtained. The comparison with experimental XANES-data is used as a criterion for the reliability of the models.

Compared to [5], where for the first time a XANES calculation for amorphous $Fe_{80}B_{20}$ was presented, an essential advantage of the present study is the presence of two absorption edges, namely the Fe–K- and the Zr–K-edge, which could be compared with calculations based on the same model.

2. Modelling

The fundamental for any XANES-calculation is the short range order around the X-ray-absorbing atoms. The strategy of the XANES calculation is described in detail in [5]. In the following, four models of amorphous $Fe_{90}Zr_{10}$ were used as a base for XANES-calculations.

2.1 *Brandt-Kizler-Models*

Three models were generated with the computer code developed by Brandt and Kronmüller [6]. The first step of the code consists in setting up a random arrangement of 140 Zr- and 1260 Fe-atoms within a periodic cube. The second step consists in the application of a relaxation procedure to this arrangement under influence of repulsive potentials between the atoms. In a third step attractive pair potentials are introduced, and a consecutive relaxation procedure leads to the final static model structure. The potentials are higher degree parabola, similar to Morse potentials. Their depths and widths are different for the Fe–Fe-, Fe–Zr- and Zr–Zr-pairs. Note that, equivalent to full or simplified molecular dynamics calculations, during the construction no rule at all is introduced to guide the developing structure in a certain manner.

From the final arrangement the partial pair correlation functions can be calculated as well as the X-ray weighted total pair correlation function and be compared with experimental data. The results are presented in Figs. 1 to 4. Since experimental data for the partial Zr–Zr-correlation function are not available, the parameters of the potentials had to be proved for a related amorphous system which permitted verification of all resulting partial pair correlation functions. For this purpose the partial pair correlation functions for the amorphous alloy $Ni_{64}Zr_{36}$ could be used [7]. Based on these data, the parameters of the potentials in the program were adjusted until the

Reprint requests to Prof. Dr. S. Steeb, Max-Planck-Institut für Metallforschung, Institut für Werkstoffwissenschaften, Seestraße 92, D-7000 Stuttgart 1.

0932-0784 / 89 / 0100-0007 $ 01.30/0. – Please order a reprint rather than making your own copy.

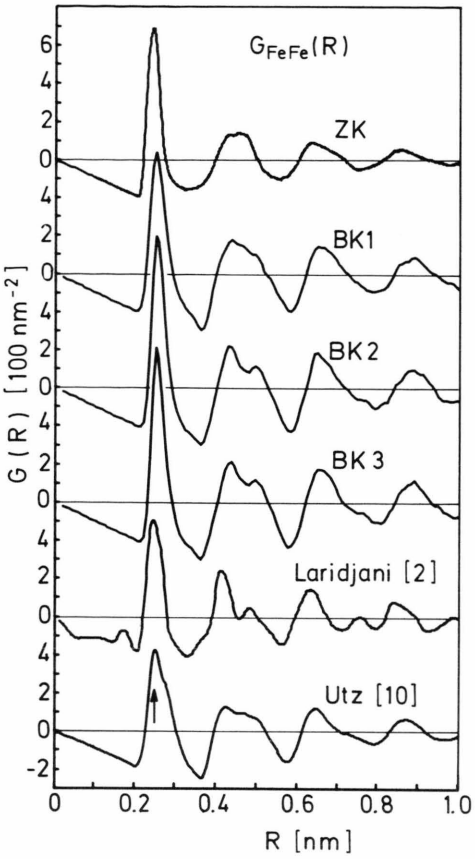

Fig. 1. Amorphous $Fe_{90}Zr_{10}$; Fe–Fe partial pair correlation functions.

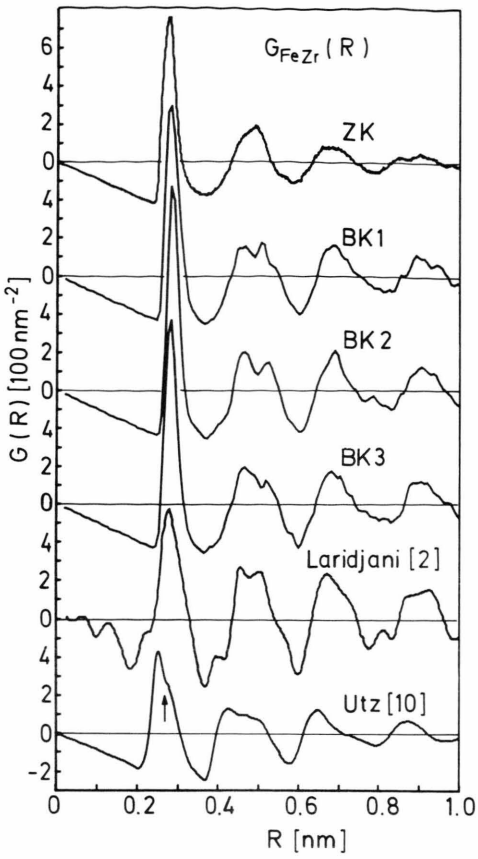

Fig. 2. Amorphous $Fe_{90}Zr_{10}$; Fe–Zr partial pair correlation functions.

models' pair correlation functions agreed well with the experimental ones for $Ni_{64}Zr_{36}$. After this adjustment, the construction of the model BK1 for the $Fe_{90}Zr_{10}$-alloy in agreement with the experimental data was possible without difficulties. Finally the interatomic pair potentials were changed to some extent in an arbitrary way in order to obtain slightly different models. The present models "Brandt-Kizler 2 and 3" arose from this variation and are abbreviated as BK2 and BK3 in the following.

The scaling of the potentials is arbitrary without reference to experimental pair potentials. The attractive Fe–Fe-pair potential for model 1 was three times as deep as for the models 2 and 3. For the attractive Fe–Zr-potential the relative depths for the models 1, 2, and 3 amounted to 5:3:2 and were much weaker than the Fe–Fe potentials. The Zr–Zr-pair potentials for all three models were very weakly attractive. A more detailed discussion of the potentials will not be given here because conclusions on the atomic structure of the models cannot be drawn from them.

2.2 Zweck-Krauss-Model

For the construction of this model 1800 Fe- and 200 Zr-atoms are distributed on the vertices of a b.c.c. lattice [8, 9]. Afterwards they are shifted from this position in a random direction by a certain distance. Finally a relaxation procedure is performed, too, under the influence of Lenard Jones potentials and with periodic boundary conditions. The parameters for the potentials in this case were chosen according to data from literature (for details see [9]). This model will be abbreviated as ZK in the following.

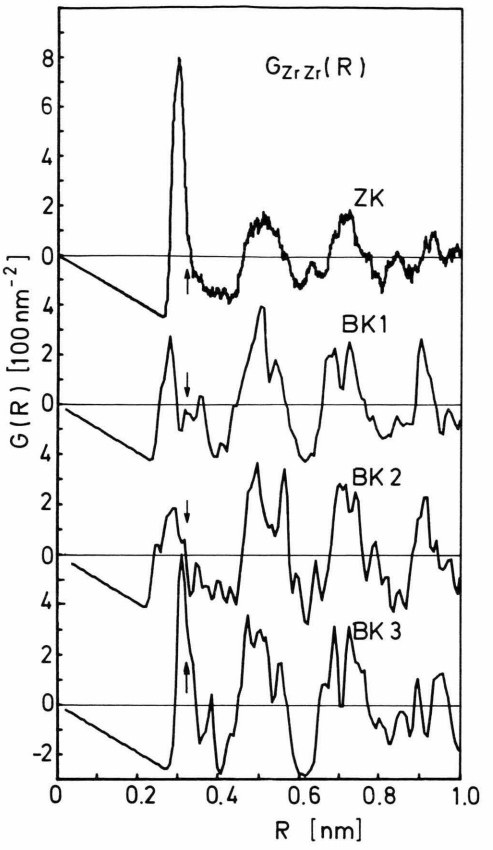

Fig. 3. Amorphous $Fe_{90}Zr_{10}$; Zr–Zr partial pair correlation functions.

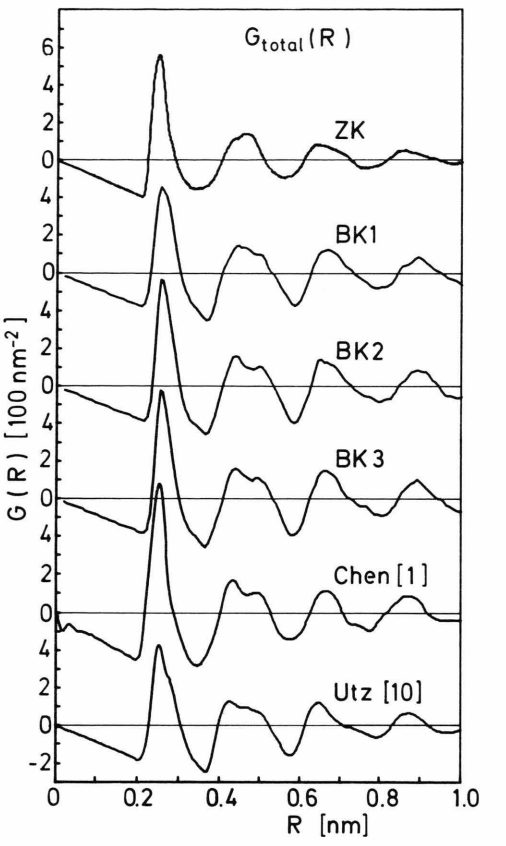

Fig. 4. Amorphous $Fe_{90}Zr_{10}$; total pair correlation functions

3. Structural Properties of the Models for Amorphous $Fe_{90}Zr_{10}$

3.1 Pair Correlation Functions from Models and Comparison with Experiments

In this chapter the partial and total pair correlation functions obtained from the models and the experiments are compared. In Fig. 1 the partial G_{FeFe} functions from the models are shown together with the experimental result as obtained by anomalous X-ray diffraction [2]. A total $G(R)$-curve obtained by energy dispersive X-ray diffraction (EDXD) [10] is also included, the first peak of which is attributed to the Fe–Fe-distance. It must be noted that in reference [2] a sample has been investigated which was prepared by vapour quenching, whereas all other experimental data were obtained with liquid-quenched samples. Possible small structural differences between samples obtained by vapour- and liquid-quenching, respectively, cannot be considered here because no comparative investigation with the same method has been performed up to now.

Figure 2 shows the partial G_{FeZr}-curves. In the total $G(R)$-curve from [10] the Fe–Zr-distance appears as a shoulder at the right hand side of the main peak.

For the partial G_{ZrZr}-curves shown in Fig. 3, no experimental data are available. The arrows indicate the Zr–Zr-distance determined for the amorphous $Ni_{64}Zr_{36}$-alloy [7]. The calculated curves in Fig. 3 are more noisy due to the small number of Zr-atoms in the models.

Figure 4 shows the total pair correlation functions for the models, which were calculated as sum of the partial ones after multiplication with the proper X-ray weighting factors. Experimental total pair correlation functions again serve for comparison. Note that scaling in Fig. 4 is different from that in Figs. 1 to 3 because

Table 1. Total and partial distances, coordination numbers and densities. (* = obtained from fitting algorithms.)

	Ref.	Distances [nm]				Coordination numbers				Density
		R_{FeFe}	R_{FeZr}	R_{ZrZr}	R_{total}	N_{FeFe}	N_{FeZr}	N_{ZrFe}	N_{ZrZr}	[g/cm³]
1) Experiment										
$Fe_{90}Zr_{10}$	[2]	0.252	0.283	–	–	10.2	1.6	14.5	–	–
$Fe_{90}Zr_{10}$	[1]	–	–	–	0.263	–	–	–	–	7.71
$Fe_{83}Zr_{17}$	[1]	0.263*	0.269*	–	0.263	11.6*	1.3*	8.4*	–	7.69
$Fe_{90}Zr_{10}$	[10]	0.250*	0.285*	0.315*	0.250	8.2*	1.6	16.1*	–	–
$Ni_{64}Zr_{36}$	[7]	0.252	0.267	0.328	–	not meaningful here				–
$Fe_{90}Zr_{10}$	this work									7.78
α-Fe	[11] [12]	0.247								7.87
2) Models										
Brandt-Kizler (BK1, BK2, BK3)	this work	0.252	0.282	0.28–0.31 noisy	0.252	12.3	1.6	13.6	1.3	7.91
Zweck-Krauss (ZK)	[9]	0.246	0.277	0.302	0.247	12.8	1.6	14.2	1.5	7.79

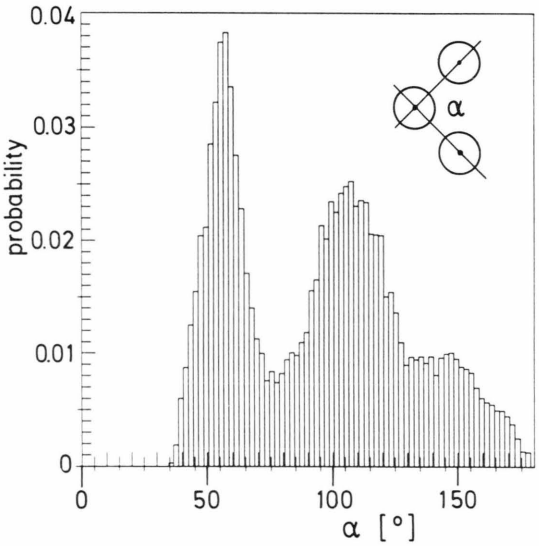

Fig. 5. Amorphous $Fe_{90}Zr_{10}$. Brandt-Kizler model BK 3. Bond angle distribution.

it is adjusted to the curve copied from the publication [1].

Concerning the partial and total pair correlation functions of the ZK model, some differences within the range of the second peak compared to the experimental function have been noted already in [9]. The main purpose for the construction of this model was to obtain a data set for the calculation of electronic and magnetic properties.

In Table 1 the atomic distances and coordination numbers obtained from the curves in Figs. 1 to 4 are compiled together with the densities.

The partial Fe–Fe coordination numbers as obtained from the models are higher than the experimental ones, whereas within the experimental uncertainties for the other pair coordination numbers no significant differences can be stated. The densities of the models agree quite well with the experimental densities.

3.2 Angular- and Coordination Number-Distribution Functions of the Models

From Figs. 1 to 4 it can be seen that among the models' pair correlation functions there are certain differences, which for the Brandt-Kizler models are small and not systematic. Concerning the differences between the G_{ZrZr}-curves we note the uncertainties due to the statistical noise. We will show later on that the model structures produce differences in the XANES calculations which in contrast to those in $G(R)$-functions are systematic. Therefore in the following further comparisons between the models are performed:

Several bond angle distributions were calculated from the different models. In [13] this has already been reported for amorphous $Fe_{80}B_{20}$. Figure 5 shows as an example the bond angle distribution for Fe–Fe–Fe-triplets for model BK 3. The bond angle distributions for the other models are almost identical to that in Figure 5.

Another interesting feature of the short range order is the distribution of the partial coordination number around its average value. Figure 6 shows the probability to meet certain coordination numbers N_{FeFe}

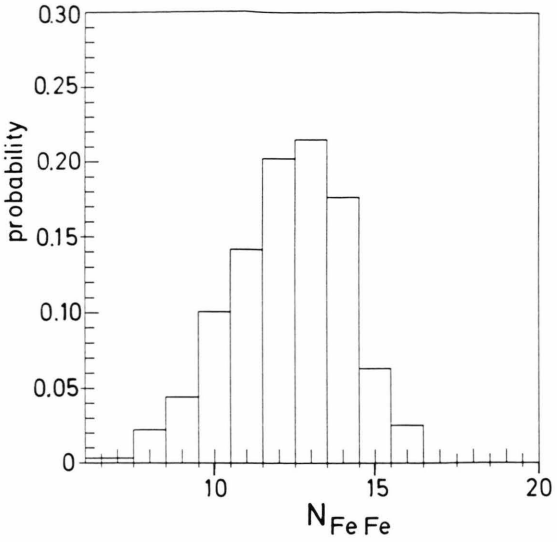

Fig. 6. Amorphous $Fe_{90}Zr_{10}$. Brandt-Kizler model BK 3. Abundance of coordination numbers N_{FeFe}.

within the first coordination sphere in model BK 3. It can be seen that the coordination number varies by a large amount from atom to atom. The existence of a distribution of coordination numbers also has been concluded from Moessbauer spectroscopy with amorphous $Fe_{90}Zr_{10}$ [14, 15, 16]. Also the coordination numbers N_{FeZr}, N_{ZrFe} and N_{ZrZr} showed a rather broad distribution.

Concerning the comparison between the different structural models is should be noted that these distributions of the coordination numbers did not exhibit any significant differences. Therefore we conclude that the systematic differences between the structural models, as shown later by XANES, have to be associated with rather hidden aspects, which cannot be investigated with the relatively simple distributions in Figs. 5 and 6.

4. Experiments

4.1 Preparation of Samples

Ribbons of amorphous $Fe_{90}Zr_{10}$ were prepared by melt spinning [17, 18] as 10 mm wide ribbons 25 μm thick. By X-ray diffraction and by transmission electron microscopy they were proved to be amorphous. Samples for the XANES measurements at the Fe–K-edge where thinned to their optimum thickness of 7 μm with a sputtering device in the etching mode.

Crystalline Fe_2Zr for a reference measurement was melted from the pure elements in an electron beam furnace under high vacuum. This alloy is very brittle and cannot be rolled to a foil as specimen for the X-ray absorption measurements. Therefore for this purpose the alloy was filed to powder and mounted on several layers of adhesive tape above each other in order to ensure sufficient homogeneity over the area of the sample. The powder was also checked by X-ray diffraction and found to be free of oxides.

4.2 XANES Measurements

The XAS measurements at the Fe–K-edge were performed in transmission mode at a laboratory XAS set up [19], which uses the bremsstrahlung of a RIGAKU rotating anode generator as radiation source. Monochromatization is done with a LiF(220) crystal monochromator. In the XANES energy range the primary beam is free of emission lines. The energy resolution was determined from the spectroscopy of a Tungsten emission line nearby the XANES energy range and was found to be $\Delta E = 7$ eV, which is a little narrower than the expected width of the structural features in the XANES curve. Due to the poor energy resolution the curve is slightly depressed close to the Fe edge.

The measurements at the Zr–K-edge were performed also in transmission at the working stations ROEMO and ROEMO II at the synchrotron radiation laboratory of Deutsches Elektronensynchrotron, DESY. The double monochromators were equipped with Si(220) crystals and have an energy resolution of $\Delta E = 6$ eV. The spectra could be recorded with very good signal to noise ratio and a measuring time of a few seconds per energy step.

Besides the as-quenched state of the $Fe_{90}Zr_{10}$ alloy also heat treated and hydrogen doped material was investigated by XANES in the present study.

The structural relaxation process of this material has also been investigated by the highly sensitive tracer diffusion method [17, 20]. It was found that a heat treatment of 10 ksec at 673 K leads to a fully relaxed state of the system. A heat treatment for longer time or at higher temperature would initiate crystallization.

A further interesting state of this alloy is achieved by charging the material with hydrogen. The hydrogenization leads to a dramatic change in the magnetic properties of this alloy [21, 22].

However, it turned out that both the relaxed and the hydrogen charged samples yielded exactly the same XANES-result as the as-quenched sample.

5. XANES Calculations and Comparisons with the Experiment

The XANES calculations were performed with the updated version [23] of the XANES computer code, published some years ago by Durham et al. [24]. The atomic phaseshifts, required for the calculation, were set up with the program MUFPOT, which was developed by Pendry and co-workers [25, 26].

Before performing the XANES calculations for the structural models, the phaseshifts were checked for a case with well known structure, namely the crystalline Fe_2Zr-alloy [27]. In Fig. 7 we present the calculated XANES-curve for the Zr–K-edge in Fe_2Zr together with the experimental curve. The agreement of the structural features in the experimental and in the theoretical curve is very good. The remaining discrepancy in the overall slopes of the two curves results from the free-atom-like transition matrix element, which is involved in the XANES calculation. The available data for these factors had been calculated for pure iron and were provided by P. J. Durham. It was not possible during the present work to calculate the transition matrix element for the case of Fe_2Zr. However, since the essential features of a XANES curve are their humps and bends, not the slope, this is not a severe problem.

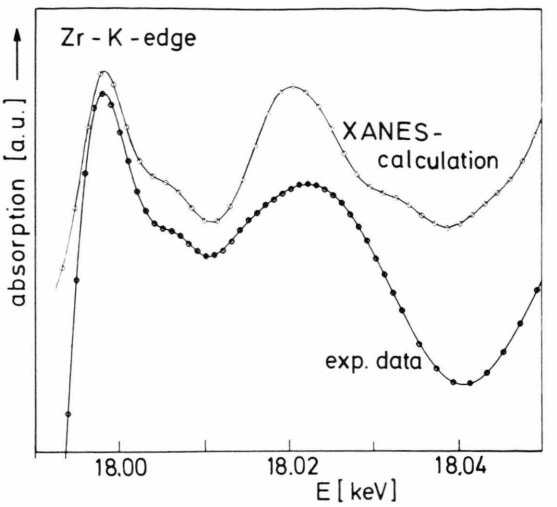

Fig. 7. Crystalline Fe_2Zr; Zr–K-edge; XANES results. Comparison between model calculation and experiment.

5.1 XANES Results at the Zr–K-edge

In Fig. 8 the calculated results for the four models are presented together with the experimental data. It can be seen that the overall shape of the curve is quite good for each of these models. However, when going from model ZK to model BK 3 we observe that the small peak "A" is showing continuously better. Nevertheless, a better coincidence in detail would be desirable.

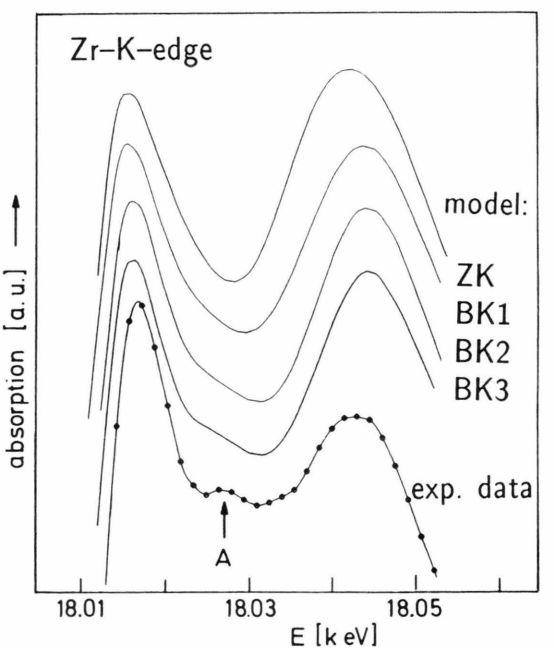

Fig. 8. Amorphous $Fe_{90}Zr_{10}$; Zr–K-edge; XANES results. Comparison between calculations for structural models and experiment.

For the purpose of a better understanding of the result, the calculations were repeated under special conditions. The computer code [23] allows certain multiple scattering paths to be switched off, thereby their individual impacts can be studied in detail.

Curves "SINGLE" and "INTER" in Fig. 9 were obtained only with single scattering calculation (SINGLE) or only with single scattering plus intershell multiple scattering, but without intrashell multiple scattering (INTER). For a definition of inter- and intrashell-multiple scattering see [23, 28]. For the "SINGLE" and "INTER" case all four models yielded the same curve. This means that the multiple scattering events, which take place in all directions, play a very important role and are essential for the understanding of the shape of the curves in Figure 8.

As was pointed out in detail in [5], the XANES result for a structural model can be calculated as the average of approximately 40 individual XANES re-

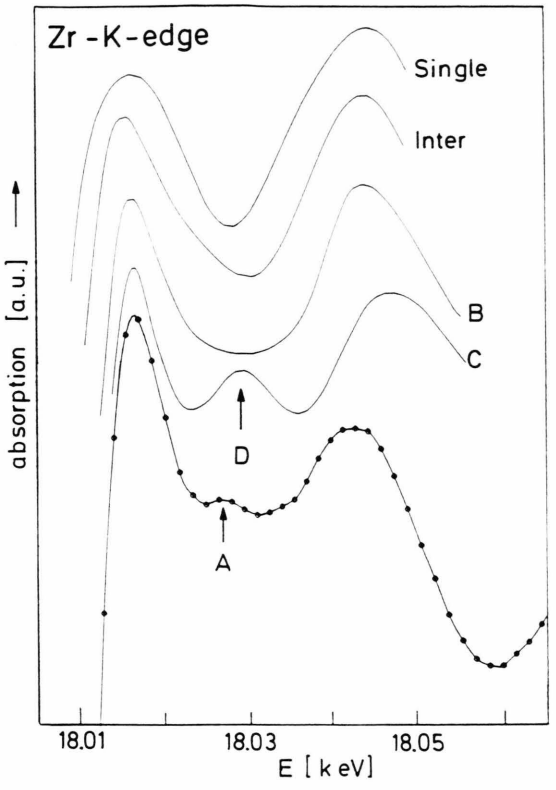

Fig. 9.
Amorphous $Fe_{90}Zr_{10}$; Zr–K-edge; XANES results. Comparison between calculations for special cases and experiment.

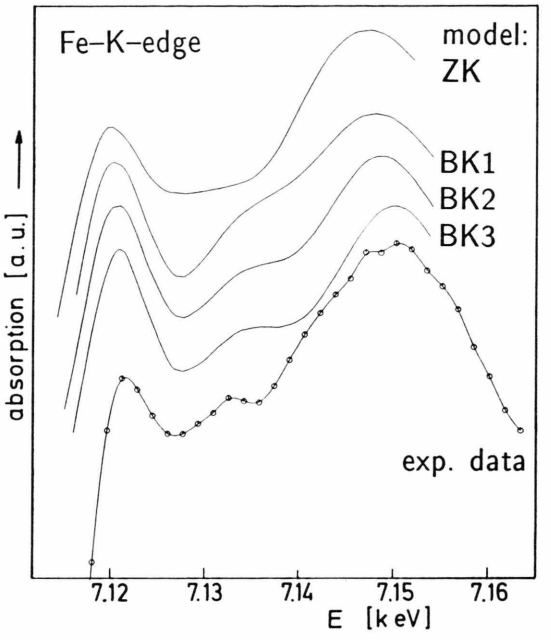

Fig. 10. Amorphous $Fe_{90}Zr_{10}$; Fe–K-edge; XANES results. Comparison between calculations for structural models and experiment.

sults for 40 individual short range orders, centered around 40 atomic sites.

The fourty single XANES curves which contribute to the result for model BK 3, were studied in detail. It was found that roughly 80% of the individual curves have a shape like curve "B", and 20% a shape like curve "C" with a pronounced peak "D". The peak "A", therefore, seems to be caused only by a minority of certain short range orders. This observation gives rise to the question whether this peculiar curvature is caused by a special kind of short range order, i.e., by the existence of special structural units in the amorphous alloy. One might also think of separation into two different amorphous phases involving different kinds of short range order. However, a detailed analysis of the atomic arrangements giving rise to curves of type B or C did not support any of these two suggestions. In some cases the existence of peak "D" depended on the existence of direct Zr–Zr neighbourhood, in other cases it did not. In some cases it depended on multiple scattering, in other cases it appeared already for single scattering calculation. So we have an example that a certain feature in a XANES curve may have very different structural reasons and must not be treated as a fingerprint of only one kind of short range order.

5.2 XANES Results at the Fe–K-edge

The results for the four models are presented together with an experimental curve in Figure 10. Like in Fig. 8 we observe a systematic change from model ZK to model BK 3, model BK 3 agreeing best, though the agreement still is not perfect.

In order to find out the reason for the differences among the curves, a calculation with single scattering this time resulted in curves which were very similar to those for full multiple scattering. This means that for the Fe–K-edge and for these models the multiple scattering processes contribute less to the differences than for the Zr–K-edge. From this follows that the details of the Fe–K-edge XANES are ruled more by the radial arrangement of the atoms.

In the case of the Fe–K-edge the 40 individual XANES curves could be sorted roughly into five categories characterized by their special features. However,

like for the case of the Zr–K-edge, a detailed analysis of the neighbourhood of the 40 central Fe-atoms did not reveal any unique relation between the XANES features and the individual short range orders.

6. Conclusion

For the $Fe_{90}Zr_{10}$ glass the applicability of the XANES method to check structural models could be shown. In addition it was shown that XANES is able to detect differences among structures which reside in higher than binary correlations.

One structural model out of four was found to agree well both with the pair correlation functions and with the XANES-curves for the Fe- and Zr–K-absorption edges.

The search for specific types of short range order as source of specific features in the XANES curves pointed to a variety of possible reasons for the individual contributing curves. This shows that treating a XANES curve as a fingerprint of a specific short range order in metallic glasses seems not to be allowed.

Acknowledgements

Thanks are due to: U. Krey, J. Zweck, and U. Krauss, University of Regensburg, F.R.G. for the numerical data of their structural model; E. H. Brandt, Max-Planck-Institut für Metallforschung, Institut für Metallphysik, Stuttgart, F.R.G. for his modelling computer code and kind introduction; Deutsches Elektronensynchrotron, DESY, Hamburg, F.R.G. for allocating beam time; B. Lengeler, KFA Jülich, F.R.G., and G. Schmiester, Free University of Berlin for their assistance during our use of the well calibrated working stations at DESY/HASYLAB; K. Pfahler, University of Stuttgart, F.R.G. for the $Fe_{90}Zr_{10}$ samples; P. J. Durham, Daresbury Laboratories, U.K. for the computer code of the original XANES program; Deutsche Forschungsgemeinschaft, Bonn, for financial support.

Special thanks are due to D. D. Vvedensky, Imperial College, London, for providing us with the updated XANES program and the MUFPOT program, kind introduction into their applications, and a lot of helpful advice.

[1] H. S. Chen, K. T. Aust, and Y. Waseda, J. Non-Cryst. Sol. **46,** 307 (1981).
[2] M. Laridjani, J. F. Sadoc, and P. Leboucher, Proc. 6th Int. Conf. on Liquid and Amorphous Metals (LAM 6), 24.–26. August 1986, Garmisch-Partenkirchen, F.R.G., Z. Phys. Chem. **157,** 17 (1988); Int. J. Mod. Phys. B **2,** 37 (1988).
[3] Workshop on Investigations of Higher Order Correlation Functions. Beyond Radial Distribution, 15.–16. July 1985, Grenoble (France), ed. by J. B. Suck, D. Quitmann, and B. Maier, J. de Physique, Colloque **C 9** (1985).
[4] P. J. Durham, J. B. Pendry, and C. H. Hodges, Sol. State Comm. **38,** 159 (1981).
[5] P. Kizler, P. Lamparter, and S. Steeb, Proc. 6th Int. Conf. on Rapidly Quenched Metals (RQ 6), Montréal (Canada), 3.–7. August 1987, Mat. Sci. Eng. **97,** 169 (1988); submitted to Z. Naturforsch.
[6] E. H. Brandt and H. Kronmüller, J. Phys. **F 17,** 1291 (1987).
[7] S. Lefebvre, A. Quivy, J. Bigot, Y. Calvayrac, and R. Bellissent, J. Phys. **F 15,** L 99 (1985).
[8] U. Krey, H. Ostermeier, and J. Zweck, Phys. Stat. Sol. (b) **144,** 203 (1987).
[9] U. Krauss, Diploma thesis, University of Regensburg, F.R.G. 1988.
[10] R. Utz, this laboratory, private communication.
[11] W. B. Pearson, Handbook of Lattice Spacings and Structures of Metals and Alloys, Pergamon Press, Oxford 1967.
[12] Landolt-Börnstein, Zahlenwerte und Funktionen, Bd. II, Springer, Berlin 1971.
[13] P. Kizler, P. Lamparter, and S. Steeb, Z. Naturforsch., in print.
[14] K. H. J. Buschow and P. H. Smit, J. Magn. Magn. Mat. **23,** 85 (1981).
[15] A. A. Kasimovskiy, Phys. Met. Metall. **60,** 150 (1985).
[16] R. Oshima, K. Nakanishi, N. S. Kazama, H. Fujimori, and F. E. Fujita, Trans. Japan Inst. Met. **25,** 772 (1984).
[17] K. Pfahler, Thesis, University of Stuttgart 1987.
[18] K. Pfahler, N. Moser, J. Horváth, W. Frank, and H. Kronmüller, Report MPI/86/P1, Max-Planck-Institut für Metallforschung 1986.
[19] S. Steeb and P. Lamparter, The Rigaku Journal **3,** 13 (1986).
[20] J. Horváth, J. Ott, K. Pfahler, and W. Ulfert, Proc. 6th Int. Conf. on Rapidly Quenched Metals (RQ 6), Montréal (Canada), 3.–7. Aug. 1987, Mat. Sci. Eng. **97,** 409 (1988).
[21] Y. Boliang, D. H. Ryan, J. M. D. Coey, Z. Altounian, J. O. Ström-Olsen, and F. Razavi, J. Phys. **F 13,** L 217 (1983).
[22] H. Fujimori, K. Nakanishi, H. Hiroyoshi, and N. S. Kazama, J. Appl. Phys. **53,** 7792 (1982).
[23] D. D. Vvedensky, D. K. Saldin, and J. B. Pendry, Comp. Phys. Comm. **40,** 421 (1986).
[24] P. J. Durham, J. B. Pendry, and C. H. Hodges, Comp. Phys. Comm. **25,** 193 (1982).
[25] J. B. Pendry, Low Energy Electron Diffraction, Academic Press, London, New York 1974.
[26] T. L. Loucks, The Augmented Plane Wave Method, Benjamin, New York 1967.
[27] K. Schubert, Kristallstrukturen zweikomponentiger Phasen, Springer, Berlin 1964.
[28] D. D. Vvedensky and J. B. Pendry, Surface Science **162,** 903 (1985).